Case Studies in Thermal Engineering 64 (2024) 105412

Contents lists available at ScienceDirect

Case Studies in Thermal Engineering

journal homepage: www.elsevier.com/locate/csite

Performance evaluation of nano-enhanced phase change materials for thermal energy storage: An experimental study

Mehmet Onur Karaağaç [a,b,*]

[a] Sinop University, Faculty of Engineering and Architecture, Department of Energy Systems Engineering, Sinop, Turkiye
[b] Sinop University, Energy Research and Application Center, Sinop, Turkiye

GRAPHICAL ABSTRACT

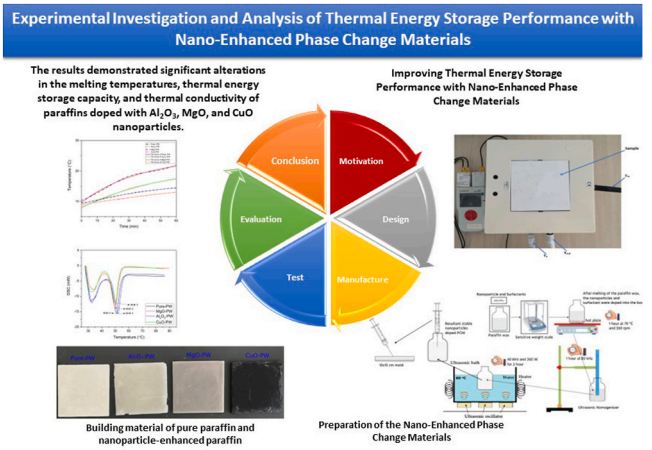

ARTICLE INFO

Handling Editor: Huihe Qiu

Keywords:
Nano enhanced phase change materials
Thermal energy storage
Nanoparticle doping

ABSTRACT

In rapidly developing economies, the increasing energy demand and fossil fuel consumption have made the need for renewable energy sources and efficient thermal energy storage (TES) solutions more urgent than ever. This study focuses on enhancing the thermal energy storage capabilities of paraffin-based phase change materials (PCMs) by incorporating Al_2O_3, MgO, and CuO nanoparticles. The evaluation of nano-enhanced PCMs focused on their melting temperatures, thermal storage capacities, thermal conductivities, and charge/discharge times. The experimental results revealed significant changes in the thermal properties of the nano-enhanced PCMs compared to

* Sinop University, Faculty of Engineering and Architecture, Department of Energy Systems Engineering, Sinop, Turkey.
E-mail address: okaraagac@sinop.edu.tr.

https://doi.org/10.1016/j.csite.2024.105412
Received 12 August 2024; Received in revised form 24 October 2024; Accepted 3 November 2024
Available online 5 November 2024

Thermal conductivity
Paraffin

pure paraffin. The melting temperature was raised by 2 °C due to Al_2O_3 nanoparticles, whereas CuO and MgO nanoparticles decreased it by 1.7 °C and 1.8 °C, respectively. Compared to pure paraffin, Al_2O_3-PW, MgO-PW, and CuO-PW exhibited improvements of 13 %, 39 %, and 48 % in thermal conductivities, respectively. CuO-doped paraffin showed an 11.8 % decrease in discharge time, suggesting its suitability for rapid heat transfer applications like defrosting systems or thermal management in electronics. On the other hand, paraffin doped with MgO showed a minimal 2.24 % reduction in discharge time, indicating its effectiveness in applications requiring heat retention, particularly for improved thermal insulation in building materials. The results highlighted the potential of nano-enhanced PCMs in energy storage and construction is underlined, offering a sustainable approach to improving energy efficiency in various sectors.

Nomenclature

T	Temperature (°C)
T_{TE}	Thermal equilibrium temperature (°C)
T_{dif}	Difference between thermal equilibrium and initial temperature (°C)
T_{up}	Upper surface temperature (°C)
W_R	The overall uncertainty value of the experimental measurements
τ	Time constant (min)
Q	Thermal energy (kJ)
W	Electrical energy input (kJ)
A	Surface area (m^2)
d	Thickness (m)
V	Voltage (V)
I	Current (A)
λ	Thermal conductivity (W/m°C)
Subscripts	
0	Initial state
Out	Outdoor
In	Indoor
Dif	Difference

1. Introduction

The importance of efficient energy utilization has steadily increased due to primary factors such as global warming caused by conventional energy technologies, diminishing resources, and escalating environmental pollution from fossil fuel use. With the advancement of technology, an increasing effort is being dedicated to addressing these challenges. In this context, utilizing the stored energy helps to reduce energy consumption and promotes more efficient usage of the resources. Therefore, this supports environmental sustainability and contributes to an extended lifespan for energy resources [1]. Recent studies have highlighted the advantages of phase change materials (PCMs) in energy storage applications [2]. PCMs are organic and inorganic materials that change phase by absorbing large amounts of heat energy. PCMs have many advantages, such as their high energy storage capacity, the capability to function across a wide temperature range, and diverse applicability in various fields [3]. PCMs have been utilized in many studies across various fields, including solar energy technology [4–7], building materials [8,9], and heat exchangers [10,11] in the literature.

The thermal performance of PCMs changes according to energy thermal conductivity, phase transition temperature, and storage density. To increase the thermal energy performance of PCMs, different methods have been used, including the integration of fins [12–15], micro and macro encapsulation [16,17], utilization of multiple PCMs [18,19], and addition of nanoparticles [20–22]. In addition to increasing the thermal efficiency of phase change materials, microencapsulation is an effective way to prevent possible interaction with the environment and leakage during the melting and solidification process [23,24]. Numerous studies focus on improving thermophysical properties by mixing nanoparticles into the base material. However, many of these studies have remained mainly at the mathematical modeling or property improvement level, with few showcasing practical application results. Paraffin, a widely used organic PCM, has attracted attention in thermal energy storage applications due to its desirable properties such as nontoxicity, cheap affordability, high latent heat storage capacity, and wide operating temperature range [25–27]. Understanding the thermal behavior of PCMs during melting and solidification in these applications is very important for different designs [28]. The thermal conductivity of paraffin material varies between 0.2 and 0.35 W/m°C. The low thermal conductivity of paraffin makes it challenging for heat to be absorbed from its surroundings and released. Consequently, this also leads to extended heat absorption and dissipation duration. The thermal performance of paraffin can be enhanced by incorporating nanoparticles with significantly higher thermal conductivity [29–31]. Materials prepared in this manner are referred to as nano enhanced PCM. Nano-enhanced PCM (NEPCM) facilitates heat storage, charging, and discharging due to increased conductivity.

With the motivation of NEPCM highlighted above, there are many reports in the literature. For instance, Shoeibi et al. combined NEPCM to enhance the efficiency of a desalination system utilized for freshwater production from saline water. The authors conducted analyses on a TES (Thermal Energy Storage) system merging paraffin wax with CuO and Al_2O_3 nanoparticles at concentrations of 0.1 % and 0.3 %, respectively. The obtained results indicated that the NEPCM with 0.3 % CuO and Al_2O_3 concentrations led to a steam efficiency increase of 55.8 % and 49.5 %, respectively. Additionally, at the 0.3 % concentration level, CuO and Al_2O_3 NEPCM exhibited

a decrease in melting temperature by 2.7 °C and 2.3 °C, respectively [21]. In another study, Zarma et al. investigated the performance of a concentrator photovoltaic nanoparticle-phase change material hybrid system. The effect of Al_2O_3, CuO, and SiO_2 nanoparticles at weight ratios of 1 % and 5 % on the overall efficiency of a concentrator photovoltaic system were examined. Nano-PCMs at a 1 % weight ratio were shown melting times of 88 min, 78 min, 80 min, and 85 min for pure PCM, Al_2O_3, CuO, and SiO2, respectively. Besides, it was found that increasing the weight fraction of nanoparticles in PCM to 5 % resulted in complete melting times of 70 min, 76 min, and 84 min for Al_2O_3, CuO, and SiO2, respectively. It is also informed that increasing the weight fraction of nanoparticles in PCM led to improved thermal conductivity and decreased melting times for Al_2O_3 and CuO NEPCMs. In addition, the authors concluded that a 5 % weight fraction produced excellent results [32]. Teng and Yu examined the heat conduction performance and thermal storage features of NEPCMs through the direct-synthesis method. The paraffin wax was mixed with alumina (Al_2O_3), titania (TiO2), silica (SiO2), and zinc oxide (ZnO) at three different concentrations: 1.0 %, 2.0 %, and 3.0 % by weight. According to the results obtained from differential scanning calorimetry (DSC) analysis, TiO_2 was found to be more effective in enhancing thermal energy storage performance compared to other additives. Furthermore, it was emphasized that when selecting the most suitable additive material, consideration should also be given to the range between phase change temperature and phase change enthalpy. However, However, the authors did not provide a complete assessment of the extent to which thermal conduction and charge-discharge times were affected [33]. Additionally, Mahdi et al. combined a triplex-tube heat exchanger with PCM and numerically investigated its thermal performance under different configurations (Al_2O_3-PCM, fins). The results obtained from the modeling revealed that adding Al_2O_3 to paraffin at concentrations of 0.1 % and 0.3 % mildly influenced the phase change rate. In contrast, the inclusion of the fin structure yielded better results [34]. In another report, Bouguila et al. proposed NEPCMs and various fin-structured heat sink models for the thermal balance of electronic devices and numerically examined them using CFD software. To identify the most effective NEPCM, they utilized graphene, CuO, and Al_2O_3 nanoparticles with 5–7% weight fractions. The numerical analyses indicated that fin variations played a role in heat conduction, while NEPCMs exhibited insulating behavior. This study was conducted through numerical modeling and required further experimental validation [35]. Approximately 40 % of the generated electricity is consumed in buildings, with 14 % of this energy being used for space heating and cooling. PCM applications in building energy systems also hold significant potential. Integrating PCMs in building walls, windows, roofs, and floors can help to reduce indoor temperature fluctuations and energy consumption for climate control. Anter et al. examined the thermal behavior of a building's wall by applying different types of PCM materials. Their results found that the indoor wall temperature was closer to the desired levels when PCM was incorporated into the wall structure. Where PCM was not used, the indoor wall temperature was 31 °C, while with PCM utilization, this value decreased to 27.7 °C [36]. In another study, Alam et al. investigated the potential of PCMs to reduce energy consumption in residential buildings using the EnergyPlus program. As a result, the authors found that buildings integrated with PCMs reduced annual heating/cooling loads by approximately 17–23 % [37]. Ma et al. examined a PV/T integrated with Cu nanoparticle RT24 PCM. The study concluded that NEPCM exhibited higher melting and solidification rates than pure PCM. Furthermore, the authors demonstrated that NEPCM stored 8.3 % more heat than pure PCM, emphasizing the need for further research to examine the mechanisms behind this enhanced performance [38]. Table 1 summarizes the changes in PCM thermal conductivity resulting from adding various nanoparticles, as reported in the literature.

PCMs can contribute to sustainability goals by improving performance and energy efficiency in areas as diverse as buildings, heat exchangers, electronic devices, and thermal energy storage. Therefore, this study aims to develop an innovative thermal energy storage material based on organic PCM, paraffin, by adding different nanoparticles to provide higher thermal conductivity and faster charging/discharging properties. The novelty of our study lies in its comprehensive experimental investigation of paraffin-based NEPCMs using three distinct nanoparticles: Al_2O_3, MgO, and CuO. While previous studies have focused on the theoretical modeling of nano-enhanced PCMs, this work advances the field by providing practical, experimental insights into how different nanoparticles

Table 1
Paraffin thermal conductivity changes by the addition of nanoparticles.

	Phase change materials		Nanometer-sized materials			
References	Material used	Phase change temperature	Materials used	Fraction	Size	findings
[39]	Paraffin	58–60 °C	Copper particles	2 wt%	25 nm	Thermal conductivity increased by 14 % in the solid state.
[40]	Paraffin	28.81 °C	Graphite particles	1, 4, 7, and 10 wt%	35 nm	The thermal conductivity found an increase ranging from 4 % to 167 %.
[41]	Paraffin	52–64 °C	Carbon nanofibers (CNFs)	1, 2, 5, and 10 wt%	Average outer diameter: 200 nm	Exhibited an increase in thermal conductivity by 24–40 %
[42]	Paraffin	58.2 °C	CuO	2, 5, and 10 wt%	40 nm	the thermal conductivity enhances 6–7.8 % in the liquid state.
[43]	Paraffin	20–25 °C	alumina (Al_2O_3) and Carbon Black (CB)	1 wt%	10–170 nm	The thermal conductivity decreased by around 7–8% with alumina nanoparticles, while it increased by 24–34 % with carbon black nanoparticles.
[44]	Paraffin	60.42 °C	Cu	0.5, 1, 1.5, and 2 wt%	20 nm	The thermal conductivity of Cu–PCM nanocomposites increased by 14.0 %, 23.9 %, 42.5 %, and 46.3 % with the dispersion of 0.5 %, 1.0 %, 1.5 %, and 2.0 % weight of nano Cu in the PCM, respectively.

affect thermal conductivity, melting points, and charge/discharge times. While Al_2O_3 and CuO nanoparticles have been extensively studied, using MgO nanoparticles in paraffin-based PCMs has been less investigated. Our work includes MgO nanoparticles, providing new insights into their potential benefits and performance characteristics in thermal energy storage applications. Samples prepared by adding 5 % by weight of Al_2O_3, CuO, and the relatively less-utilized MgO nanoparticles to paraffin with a melting temperature of around 52 °C have been experimentally investigated. In this context, analyses have been conducted to reveal the differences between NEPCMs and pure paraffin. Furthermore, comprehensive comparisons were conducted by subjecting the obtained NEPCMs to discharge processes under constant environmental conditions. By introducing MgO nanoparticles, which have been relatively less investigated, our study provides new insights into their potential benefits and performance characteristics in thermal energy storage applications. The development of these materials aims to contribute to the development of efficient energy storage solutions while minimizing environmental impacts.

2. Materials and methods

2.1. Materials

This study chose paraffin as the reference material due to its easy availability, non-toxic nature, and organic composition. However, the low thermal conductivity of paraffin presents a disadvantage. High thermal conductivity nanoparticles, Al_2O_3, CuO, and MgO, were added in a weight ratio of 5 % to enhance PCM thermal conductivity. The selection of the 5 % additive ratio was made to significantly raise paraffin's thermal conductivity while simultaneously preserving the energy storage capacity of the phase change material. Higher proportions of additives could potentially lead to agglomeration, induce defects in the lattice structure, and risk the energy storage capacity. Thus, the 5 % ratio can be considered an effective balance point for enhancing thermal conductivity without compromising energy storage capabilities. Research has indicated that higher proportions of additives may lead to a trade-off between enhanced thermal conductivity and energy storage capabilities [29,45–47]. Therefore, the 5 % weight ratio was knowingly chosen to optimize the thermal performance of the paraffin-based PCM while preserving its energy storage characteristics. The reasons for the selection of Al_2O_3, CuO, and MgO are based on their various physical and chemical properties. Al_2O_3 is known for its high thermal conductivity and chemical stability [29,48]. CuO, in addition to having high thermal conductivity, possesses an appropriate energy storage capacity [32,49,50]. MgO offers both high thermal conductivity and a favorable price-performance balance [51,52]. The choice of these nanoparticles was made carefully to ensure the best balance between high thermal conductivity and suitable energy storage capacity. In other words, Al_2O_3, CuO, and MgO were selected as suitable options for achieving the best balance in terms of both thermal conductivity and energy storage capacity.

The technical specifications of the nanoparticles used are presented in Table 2. The comparison was conducted in order to evaluate the effects of these additives. For the production of Nano-Enhanced Phase Change Materials, the additives were combined with paraffin through the direct synthesis method. The procedure of this process is illustrated in Fig. 1.

2.2. Preparation of the NEPCM

The nanoparticles, surfactants, and PCM material were weighed with ±0.01 g accuracy on a sensitive balance. Subsequently, the PCM material was melted on a heating plate at 70 °C. After melting the PCM, nanoparticles were introduced into the molten material at a concentration of 5 wt%. In addition, surfactants were added in quantities proportional to the nanoparticle mass. Following this step, the nanoparticle-PCM mixture was thoroughly stirred on the heated plate using a mixer set at 70 °C and 550 rpm for 1 h. Then, the mixer was replaced with an ultrasonic homogenizer, and the mixture was processed at 20 kHz for 1 h. It is essential to note that excessive heating of the mixture should be avoided. For further enhancement of the features, the mixture was exposed to a power of 260 W and a frequency of 40 kHz in an ultrasonic bath at 60 °C for 3 h. Subsequently, a PCM material containing stable nanoparticles was obtained. At this stage, the sample remained in the liquid phase, allowing the prepared nano-FDM sample to be injected into the mold made of a metal plate. In the final step, the sample was allowed to solidify within the mold under laboratory conditions (~20 °C). A portion of the remaining sample was used for DSC measurements. A PCM material containing stable nanoparticles was obtained for the experiments. Images of the obtained samples, sized at 10x15, removed from the mold, are shown in Fig. 2.

2.3. DSC analysis

The prepared samples undergo thermal analysis through Differential Scanning Calorimetry (DSC) measurements. The DSC technique is commonly employed for determining quantitative energy changes [53]. The fundamental principle of DSC analysis is to

Table 2
Technical properties of nanoparticles.

Nanoparticle	Purity (%)	Average Particle Size (nm)	Specific Surface Area (m^2/g)	True Density (g/cm^3)	Thermal conductivity (W/m K)	Heat capacity (kJ/kg K)	Density (kg/m^3)
Al_2O_3	99.5	78	>20	3.9	40	765	3970
CuO	99.99	45	15.0	6.5	18	540	6510
MgO	99.95	45	>45	3.6	42	877	3580

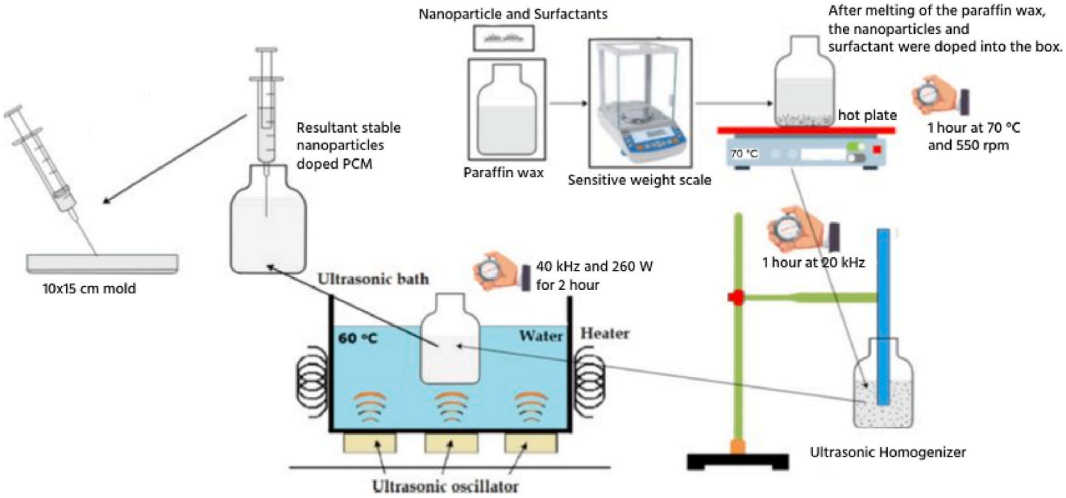

Fig. 1. Preparation of NEPCM using the direct synthesis method.

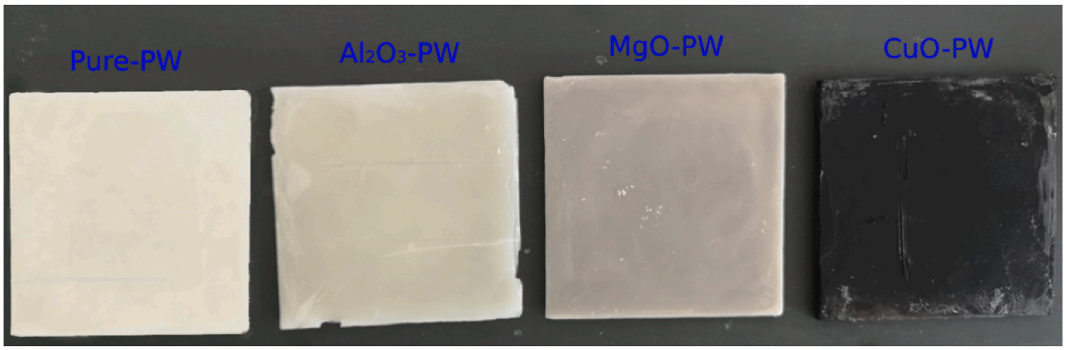

Fig. 2. Samples of pure paraffin and nanoparticle-enhanced paraffin.

prevent temperature differences between the sample and the reference. Therefore, DSC measures the energy applied to the sample or reference to ensure their temperatures remain identical. The technical specifications and analysis conditions of the employed DSC apparatus are presented in Table 3.

The graphs of DSC measurements for the reference sample, paraffin, and the Al_2O_3, CuO, and MgO-doped NEPCMs are illustrated in Fig. 3. Furthermore, the thermal findings derived from these curves are presented in Table 4.

As shown in the graph, the first peak temperatures for pure paraffin, Al_2O_3-doped paraffin, CuO-doped paraffin, and MgO-doped paraffin were determined as 31.79 °C, 32.72 °C, 32.64 °C, and 34.06 °C, respectively. Solid-solid phase transitions occurred here, and latent heat energies of 97.9 kJ/kg, 95.1 kJ/kg, 77.3 kJ/kg, and 62.1 kJ/kg were respectively observed. While the second peak temperature for pure paraffin was 50.95 °C, for Al_2O_3-doped paraffin, CuO-doped paraffin, and MgO-doped paraffin, it was determined as

Table 3
Technical specifications of the DSC Analyzer and thermal analysis conditions.

Technical specifications of the DSC analyzer	
Manufacturer	HITACHI DSC7020
Temperature range	−150–725 °C
Crucible	Alumina
Heat range	±350 mW
Accuracy	0.2 μW
Ramp rate	0.01–100 °C
Thermal Analysis Conditions	
Quantity of sample	7–8 mg
heating rate	2 °C/min.
Temperature range	25-80 °C

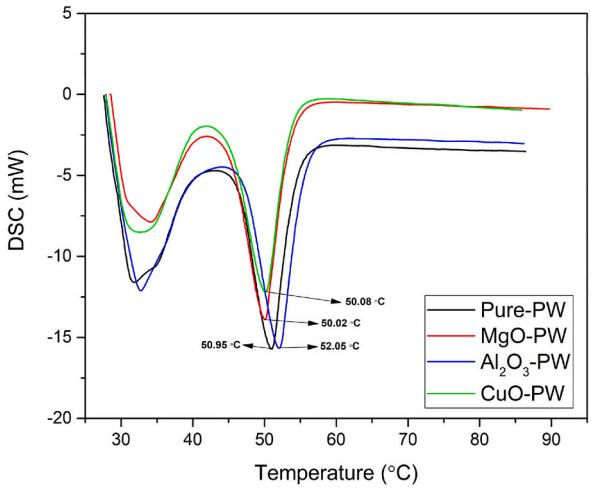

Fig. 3. DSC curves of the prepared samples.

Table 4
Paraffin wax and NEPCMs thermal properties.

Parameter	Paraffin wax	Al_2O_3-NEPCM	CuO-NEPCM	MgO-NEPCM
the first peak, °C	31.79	32.72	32.64	34.06
the second peak, °C	50.95	52.05	50.08	50.02
The total latent heat (L), (kJ/kg)	360	339	322	310

52 °C, 50.08 °C, and 50.02 °C, respectively. A solid-liquid phase transition (melting) occurred here, resulting in latent heat energies of 262 kJ/kg, 244 kJ/kg, 245 kJ/kg, and 248 kJ/kg, respectively. Adding Al_2O_3, CuO, and MgO nanoparticles to paraffin led to changes in melting points. While Al_2O_3 nanoparticles caused a 2 % increase in melting temperature, CuO and MgO nanoparticles caused reductions of 1.7 % and 1.8 %, respectively. The total latent heat storage capacities of pure paraffin and Al_2O_3, CuO, and MgO nanoparticle doped NEPCMs were found to be 360 kJ/kg, 339 kJ/kg, 322 kJ/kg, and 310 kJ/kg, respectively. Incorporating Al_2O_3, CuO, and MgO nanoparticles reduced thermal energy storage capacities by 5.8 %, 10.4 %, and 13.8 %, respectively.

3. Experimental analysis

3.1. Thermal conductivity analysis

The obtained samples underwent the single-plate method analysis to calculate the thermal conductivity and performance tests were conducted in a sample application. The single-plane method is a heat transfer experiment used to determine a material's thermal conductivity, which indicates its ability to heat transfer [54]. This characteristic is crucial for energy efficiency and thermal storage. In this experiment, one side of the specimen is heated by heat source, while the other surface is maintained at a lower temperature. Heat

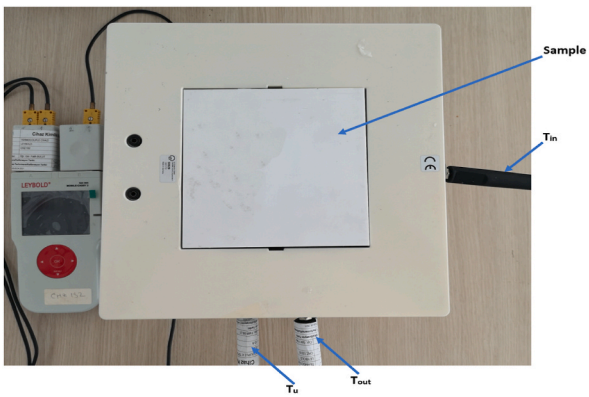

Fig. 4. System for determining the thermal conductivity of materials using the single plate method.

flows from the hot lower plate to the colder upper plate. The sample's thermal conductivity can be calculated by measuring the temperature difference of the sample and knowing its dimensions and applied heat.

For these experiments, an open-top chamber with dimensions of 28x28 × 20 cm was utilized. This chamber is a double-walled insulated box with suitable insulation material between the walls. Temperature measurements were conducted within the chamber in order to assess the performances of pure paraffin and NEPCMs. In this setup, the prepared samples were placed on the upper side, and an electric heater was connected inside the box to provide heat. The schematic representation of the experiment is shown in Fig. 4. In order to assess the reliability of the experimental setup, a conductivity check was performed using a well-known material, Fermacell (gypsum). The thermal conductivity value of Fermacell, obtained from the manufacturer, was approximately 0.27 W/m°C. The experimental result yielded a thermal conductivity of 0.28 W/m°C. Consequently, the error margin of the experimental system was determined to be 3.7 %. The conducted validation process using a known material has established the accuracy and precision of the experimental apparatus, thereby ensuring the reliability of the obtained results. The equipment specifications are shown in Table 5.

The temperature T_{out} represents the temperature of the upper side of the sample placed in the experimental system, T_u is the temperature of the underside of the sample placed in the experimental system, and T_{in} represents the temperature of the sample's interior placed in the experimental system. T_{out} temperature was attempted to be maintained within the range of −2 to +4 °C throughout the experiment. The system is not in thermal equilibrium immediately after the heater inside the chamber is turned on. In order to obtain the temperature difference at thermal equilibrium, the temperatures are monitored and recorded for 1 h.

When a temperature difference is applied across a material, heat flow occurs, and this phenomenon is referred to as thermal conduction. Thermal conductivity is a property that indicates a material's ability to conduct heat. The single-plate method determines thermal conductivity by measuring a material's direct temperature difference and thermal flux $\Delta Q/\Delta t$ of a material with thickness d, surface area A, and thermal conductivity (λ). In other words, according to Fourier's Law of Heat Conduction, the equation for heat flux passing through a single plane is shown in equation (1):

$$\frac{\Delta Q}{\Delta t} = \lambda \frac{A}{d} \Delta T \text{ or } \lambda = \frac{\Delta Q}{\Delta t} \frac{d}{A} \frac{1}{\Delta T} \tag{1}$$

The homogeneous passage of heat through the sample and prevention of heat dissipation through other means (heat transfer to the environment) is critical for accurate measurements. The chamber is well insulated for the experiment to prevent heat loss to the environment. An electric heater is employed within the chamber to facilitate heat flow through the prepared TES materials. At the same time, a piece of ice is placed directly on the upper surface of the sample.

$$P = \frac{\Delta Q}{\Delta t} \text{ or } P.t = W = Q \tag{2}$$

Where W represents the inlet electrical energy, and Q is the flow of thermal energy in the sample. Thus, the thermal conductivity of the prepared sample can be calculated using Equation (3).

$$\lambda = P \frac{d}{A} \frac{1}{\Delta T} \tag{3}$$

The change in the temperature of the bottom surface of the sample over time, which corresponds to an increase in temperature, is directly proportional to a constant, and this relationship is shown in Equation (4) as follows.

$$\frac{\Delta T}{\Delta t} = aT + B \tag{4}$$

This equation is a function of temperature regarding time and can be calculated as shown below.

$$T(t) = T_{TE} - T_{dif}.\, e^{\frac{t}{\tau}} \tag{5}$$

Where T_{TE} , T_{dif} and τ represent the internal temperature at thermal equilibrium, the difference between the thermal equilibrium temperature and the initial temperature of the sample $(T_{dif} = T_{TE} - T_0)$, and the time constant. This equation can be written as

Table 5
The equipment used in the system.

Equipment Name	Properties
Thermocouple Device	Leybold Mobile-CASSY 2 WiFi Measuring range Temp: −200 … +200 °C/−200 … +1200 °C Sampling rate: max. 500,000 values/second Resolution: 12 bit Dimensions: 75 mm × 95 mm x 40 mm
Temperature Probe	NiCr-Ni Type K Measuring range: −50 °C … 1100 °C Reaction time: 0.9 s Precision: ½ DIN IEC 584 class 2 (±1.25 %) Probe length: 190 mm Probe diameter: 1.5 mm, flat tip Cable length: 2 m

equation (6) below by adapting the time-dependent sub temperature graph recorded throughout the experiment.

$$f(x) = A - B.e^{\frac{-x}{C}} \tag{6}$$

Parameter A in this adapted equation corresponds to the thermal equilibrium temperature (T_{TE}) value we want to obtain. Ice placed on the top of the sample keeps the outside temperature low and as constant as possible. Since there may still be small temperature fluctuations, the Upper-temperature values are averaged and included in calculating this average temperature difference. The thermal conductivity coefficient can be calculated using equation (3).

$$\Delta T = \left(T_{TE} - T_{up}\right) \tag{7}$$

The experiments were conducted by placing flat, homogeneous specimens between two temperature-controlled plates. The experiment is conducted under steady conditions, and the single plate heat transfer changes over time in lower specimen temperatures are shown in Fig. 5. The results obtained by adapting the temperature-time graph to obtain the thermal equilibrium temperature are presented in Table 6. The thermal equilibrium temperature for pure paraffin was calculated as 24.57 °C, while the thermal equilibrium temperatures for Al_2O_3, MgO, and CuO for NEPCMs were calculated as 22.12 °C, 17.8 °C and 16.1 °C, respectively.

The thermal conductivity of the TES materials was calculated by obtaining the thermal equilibrium temperature from the underside temperature curves and averaging the upper temperature values. Besides, the results are shown in Table 7. As seen from the table, the thermal conductivities of Pure-PW, Al_2O_3-PW, MgO-PW, and CuO-PW were calculated 0.22 W/m°C, 0.26 W/m°C, 0.34 W/m°C, and 0.36 W/m°C, respectively. It is observed that Al_2O_3, MgO, and CuO nanoparticle-doped kinds of paraffin have thermal conductivities of 13 %, 39 %, and 48 % higher than pure paraffin, respectively.

Table 1 summarizes the changes in PCM thermal conductivity resulting from adding various nanoparticles, as reported in the literature. While there is no direct resemblance between the current study and those found in the literature, a certain parallelism exists. This differentiation may stem from various factors, such as variations in the type of paraffin employed, preparation procedures for the mixture, and differences in the size and characteristics of the nanoparticles utilized. In this study, compared to pure paraffin, paraffin with Al_2O_3, MgO, and CuO nanoparticle additives exhibited respective improvements of 13 %, 39 %, and 48 % in thermal conductivity.

3.2. Uncertainty analysis

The overall uncertainty value of the experimental investigation was computed using the subsequent equations. This formulation signifies the overall uncertainty of the study in terms of percentage, while and represents the uncertainty function and the dimensional factor, respectively. Additionally, within the same equation, denotes the uncertainties expresses in the independent variables [55].

$$W_R = \left[\left(\frac{\partial R}{\partial x_1} w_1\right)^2 + \left(\frac{\partial R}{\partial x_2} w_2\right)^2 + \ldots \left(\frac{\partial R}{\partial x_n} w_n\right)^2\right] \tag{8}$$

The overall uncertainty associated with this research, as determined from measurements obtained using thermocouples, was found to be 1.50 %. The total uncertainty value being below 5 % highlights the reliability and acceptability of the tests conducted.

3.3. Thermal energy storage analysis

The prepared materials were subjected to a practical application to assess their thermal energy storage performance. In this experiment, using the same chamber, the prepared samples were heated to 70 °C to transition into the liquid phase, followed by

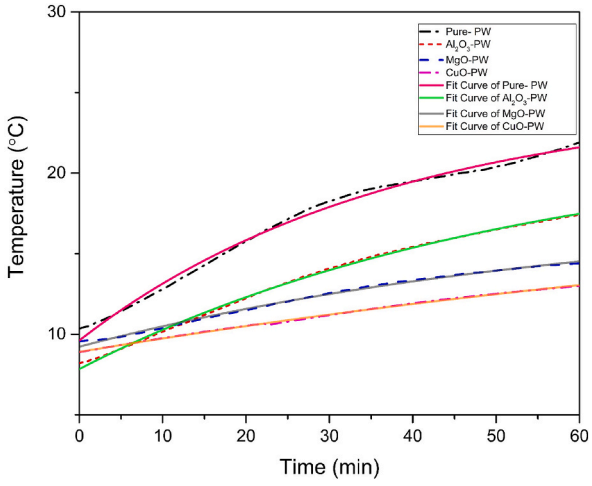

Fig. 5. Time-dependent graph of temperatures of the underside of the pure paraffin and NEPCMs samples.

Table 6
Curve fitting results of temperature time graph.

Equation	y = A1*exp(-x/t1) + y0			
Plot	Pure- PW	Al_2O_3-PW	MgO-PW	CuO-PW
y0	24.5759 ± 0.1731	22.1277 ± 0.1269	18.8037 ± 0.1579	17.1055 ± 0.0254
A1	−14.9631 ± 0.1458	−14.2910 ± 0.1150	−8.5788 ± 0.1466	−7.8441 ± 0.0247
t1	37.1803 ± 0.8875	53.4369 ± 0.8020	62.5289 ± 1.8124	64.2182 ± 0.3382
R-Square (COD)	0.9945	0.9988	0.9969	0.9991

Table 7
Heat conduction calculation.

	Pure- PW	Al_2O_3-PW	MgO-PW	CuO-PW
A (m2)	0.0225			
d (m)	0.01			
V (V)	12			
I (A)	1			
T_E (°C)	24.50	22.10	18.80	17.10
T_u (°C)	1.76	1.53	2.15	1.44
ΔT (°C)	22.74	20.57	16.65	15.66
λ (W/m°C)	0.23	0.26	0.32	0.34

monitoring the temperature changes of both the sample and the chamber. These experiments were conducted in a cold room at a constant temperature of 5 °C. The solidification curve obtained from these experiments is illustrated in Fig. 6, while the temperature variation of the chamber throughout this process is depicted in Fig. 7. The internal temperature shown in Fig. 6 represents the temperature of the paraffin, while the outdoor temperature in Fig. 7 represents the temperature of the closed chamber where the paraffin is located. In the thermal energy storage experiment, two thermocouples were used: one to measure the temperature of the paraffin, placed at the center of the sample, and the other to measure the temperature of the insulated chamber, positioned 4 cm above the sample surface.

In this experiment, conducted to test the time taken by paraffin and NEPCM samples to release the absorbed thermal energy, the durations for the temperature to drop from 70 °C to 35 °C were examined. While pure paraffin takes 312 min to drop from 70 °C to 35 °C, the paraffin doped with Al_2O_3, CuO, and MgO nanoparticles exhibited 285 min, 275 min, and 305 min, respectively. These results demonstrate that adding 5 wt% Al_2O_3, MgO, and CuO nanoparticles to pure paraffin material reduces the discharging time. Compared to pure paraffin, the reduction in discharging times for Al_2O_3-PW, CuO-PW, and MgO-PW was determined as 8.6 %, 11.8 %, and 2.24 %, respectively. Besides, it was found that the fastest discharging rate was achieved with CuO nanoparticle-doped paraffin.

When examining the temperature change graph of the chamber during the cooling of the prepared samples, the highest outdoor temperature was observed in the case of the pure paraffin material throughout the experiment. Following the Pure-PW, the outdoor temperature for MgO-PW, Al_2O_3-PW, and CuO-PW samples was observed. Pure-PW decreased to 22 °C at the end of the experiment, while the temperature changes observed at the end of the experiment for MgO, Al_2O_3, and CuO were 20.2 °C, 19.8 °C, and 20.2 °C, respectively. Since Pure-PW has a significantly higher thermal energy storage capacity compared to other samples, it maintained a higher chamber temperature. Additionally, MgO-PW presented a higher chamber temperature progression than Al_2O_3-doped paraffin despite its lower energy storage capacity and higher thermal conductivity. The phase change for MgO-PW was shorter than pure paraffin, followed by a rapid decrease.

4. Conclusions

In this study, organic PCM paraffin was chosen as the reference sample, and NEPCMs were experimentally investigated for their thermal energy performance by adding Al_2O_3, MgO, and CuO nanoparticles to enhance thermal conductivity. Accordingly, some analyses were conducted to reveal the differences between the obtained NEPCMs and pure paraffin. The results obtained from the study are summarized below.

- The melting temperatures of pure paraffin, Al_2O_3-doped paraffin, CuO-doped paraffin, and MgO-doped paraffin were determined as 50.95 °C, 52 °C, 50.08 °C, and 50.02 °C, respectively. The addition of Al_2O_3 nanoparticles increased the melting temperature of the paraffin material, while CuO and MgO nanoparticles caused a decrease in the melting temperature.
- The total latent heat storage capacities of pure paraffin and Al_2O_3, CuO, and MgO nanoparticle doped NEPCMs were found to be 360 kJ/kg, 339 kJ/kg, 322 kJ/kg, and 310 kJ/kg, respectively. The addition of Al_2O_3, CuO, and MgO nanoparticles to paraffin resulted in decreases in thermal energy storage capacities by 5.8 %, 10.4 %, and 13.8 %, respectively.
- In the conducted single-plate heat transfer experiment, the thermal conductivity values for Pure-PW, Al_2O_3-PW, MgO-PW, and CuO-PW were calculated as 0.22 W/m°C, 0.26 W/m°C, 0.34 W/m°C, and 0.36 W/m°C, respectively. Compared to pure paraffin, paraffin doped with Al_2O_3, MgO, and CuO nanoparticles exhibited 13 %, 39 %, and 48 % higher thermal conductivity, respectively.

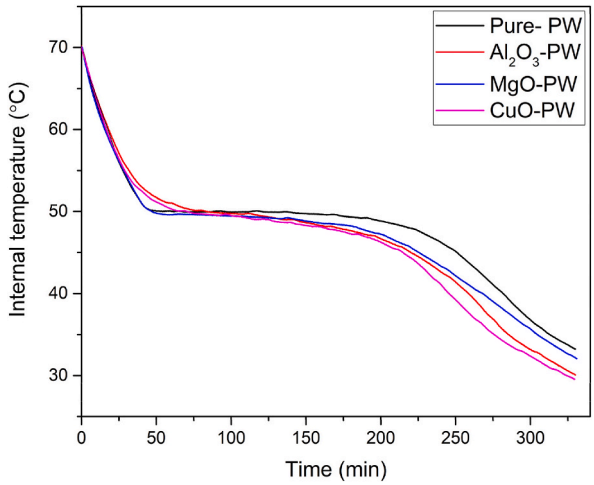

Fig. 6. Experimental solidification profile of PW and NEPCMs.

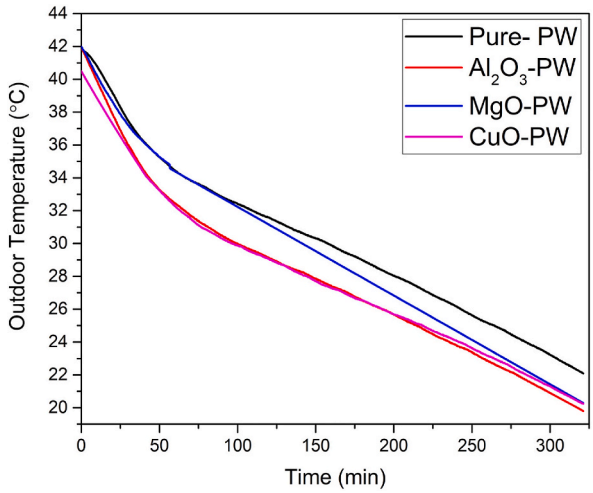

Fig. 7. Outdoor temperature variations of PW and NEPCMs.

As a result, these doped paraffins can absorb thermal energy from an external source more rapidly, enabling faster charging and discharging processes.

- Another TES experiment revealed the potential use of doped paraffins in applications requiring faster heat transfer. A comparison with pure paraffin showed that the reduction in discharge times for Al_2O_3-PW, CuO-PW, and MgO-PW were 8.6 %, 11.8 %, and 2.24 %, respectively. As a result, doped paraffins reached more rapid discharge rates than pure paraffin.

In short, this study investigated the thermal energy performance of NEPCMs created by incorporating Al_2O_3, MgO, and CuO nanoparticles into organic PCM paraffin. The results demonstrated significant alterations in the melting temperatures, thermal energy storage capacity, and thermal conductivity of paraffins doped with Al_2O_3, MgO, and CuO nanoparticles. It has been revealed that nanoparticle-doped paraffins have the potential to be used, especially in applications that require rapid heat transfer. Notably, CuO-PW substantially reduced charge and discharge times, making it promising for defrost and PVT applications. On the other hand, MgO-doped PCM might be more suitable for applications where heat preservation is crucial, such as building insulation. These findings offer insights into future developments in energy storage and thermal management. Furthermore, materials of this nature may possess higher heat storage capacities than traditional insulation materials. Adding Al_2O_3, MgO, and CuO nanoparticles can enhance heat absorption, improving thermal comfort. The results could contribute to advancing sustainable and efficient insulation solutions in the construction sector.

Declaration of competing interest

The authors declare that they have no known competing financial interests or personal relationships that could have appeared to influence the work reported in this paper.

Data availability

The authors are unable or have chosen not to specify which data has been used.

References

[1] K.Y. Leong, M.R. Abdul Rahman, B.A. Gurunathan, Nano-enhanced phase change materials: a review of thermo-physical properties, applications and challenges, J. Energy Storage 21 (2019) 18–31, https://doi.org/10.1016/j.est.2018.11.008.

[2] W.A. Dukhan, N.S. Dhaidan, T.A. Al-Hattab, F.N. Al-Mousawi, Phase-change of paraffin inside heat exchangers: an experimental study, Int. J. Environ. Sci. Technol. 19 (2022) 3155–3164, https://doi.org/10.1007/s13762-021-03367-2.

[3] M. Teggar, E.H. Mezaache, Numerical investigation of a PCM heat exchanger for latent Cool storage, Energy Proc. 36 (2013) 1310–1319, https://doi.org/10.1016/j.egypro.2013.07.149.

[4] M.O. Karaağaç, A. Ergün, Ü. Ağbulut, A.E. Gürel, İ. Ceylan, Experimental analysis of CPV/T solar dryer with nano-enhanced PCM and prediction of drying parameters using ANN and SVM algorithms, Sol. Energy 218 (2021) 57–67, https://doi.org/10.1016/j.solener.2021.02.028.

[5] B.M. Tripathi, S.K. Shukla, P.K.S. Rathore, A comprehensive review on solar to thermal energy conversion and storage using phase change materials, J. Energy Storage 72 (2023) 108280, https://doi.org/10.1016/j.est.2023.108280.

[6] B. Gao, S. Liu, A.R. Mazhar, Y. Shen, T. Chen, S. Zhang, A tree-shaped layout heat pipe to enhance heat transfer in A phase-change material storage process, JEH (T) 30 (2023), https://doi.org/10.1615/JEnhHeatTransf.2023046022.

[7] R. Jiang, M.-J. Li, W.-Q. Wang, M.-J. Li, Model development and performance improvement of A photovoltaic-thermoelectric system by integrating and optimizing phase change materials, HTR 54 (2023), https://doi.org/10.1615/HeatTransRes.2022044532.

[8] F. Simon, L. Ruiz-Valero, A. Girard, H. Galleguillos, Experimental and numerical analysis of a PCM-integrated roof for higher thermal performance of buildings, J. Therm. Sci. 33 (2024) 522–536, https://doi.org/10.1007/s11630-023-1909-5.

[9] A. Saliby, B. Kovács, Minimization of annual energy consumption by incorporating phase change materials into building components, A Comprehensive Review, HTR 54 (2023), https://doi.org/10.1615/HeatTransRes.2023047570.

[10] M. Ismail, W.K. Zahra, H. Hassan, Experimental study of vapor compression refrigeration system enhanced via tubular heat exchanger incorporating single/dual phase change materials, Case Stud. Therm. Eng. 49 (2023) 103164, https://doi.org/10.1016/j.csite.2023.103164.

[11] B.E. Kareem, A.M. Adham, B.N. Yaqob, Design and optimization of air to PCM heat exchanger using CFD, Arab J Sci Eng 48 (2023) 12609–12623, https://doi.org/10.1007/s13369-022-07360-w.

[12] M. Al-Jethelah, S. Humaira Tasnim, S. Mahmud, A. Dutta, Melting of nano-PCM in an enclosed space: scale analysis and heatline tracking, Int. J. Heat Mass Tran. 119 (2018) 841–859, https://doi.org/10.1016/j.ijheatmasstransfer.2017.11.106.

[13] H.A. Al-Salami, N.S. Dhaidan, H.H. Abbas, F.N. Al-Mousawi, R.Z. Homod, Review of PCM charging in latent heat thermal energy storage systems with fins, Therm. Sci. Eng. Prog. 51 (2024) 102640, https://doi.org/10.1016/j.tsep.2024.102640.

[14] M.J. Hosseini, M. Rahimi, R. Bahrampoury, Experimental and computational evolution of a shell and tube heat exchanger as a PCM thermal storage system, Int. Commun. Heat Mass Tran. 50 (2014) 128–136, https://doi.org/10.1016/j.icheatmasstransfer.2013.11.008.

[15] F.L. Rashid, N.S. Dhaidan, A.J. Mahdi, H.N. Azziz, R. Parveen, H. Togun, R.Z. Homod, Heat transfer enhancement of phase change materials using letters-shaped fins: a review, Int. Commun. Heat Mass Tran. 159 (2024) 108096, https://doi.org/10.1016/j.icheatmasstransfer.2024.108096.

[16] K. Bhagat, S.K. Saha, Numerical analysis of latent heat thermal energy storage using encapsulated phase change material for solar thermal power plant, Renew. Energy 95 (2016) 323–336, https://doi.org/10.1016/j.renene.2016.04.018.

[17] Y. Dong, F. Wang, L. Yang, X. Shi, G. Zhang, Y. Shuai, Thermal performance analysis of PCM capsules packed-bed system with biomimetic leaf hierarchical porous structure, J. Therm. Sci. 30 (2021) 1559–1571, https://doi.org/10.1007/s11630-021-1462-z.

[18] N. Dhaidan, H. Hashim, A. Abbas, J. Khodadadi, W. Almosawy, F. Al-Mousawi, Discharging of PCM in various shapes of thermal energy storage systems: a review, J. Therm. Sci. 32 (2023) 1124–1154, https://doi.org/10.1007/s11630-023-1793-z.

[19] K. Bhagat, S.K. Saha, Numerical investigation of entropy generation during the discharge of encapsulated phase change material-based thermal, Energy Storage, HTR 51 (2020), https://doi.org/10.1615/HeatTransRes.2019027218.

[20] A. Ergün, Energy and exergy analysis of a PV/thermal storage system design integrated with nano-enhanced phase changing material, Int. J. Exergy 32 (2020) 82–101, https://doi.org/10.1504/IJEX.2020.107745.

[21] S. Shoeibi, H. Kargarsharifabad, N. Rahbar, Effects of nano-enhanced phase change material and nano-coated on the performance of solar stills, J. Energy Storage 42 (2021) 103061, https://doi.org/10.1016/j.est.2021.103061.

[22] Y. Zhang, H. Lin, R. Chaturvedi, P.K. Singh, I.B. Mansir, K. Zhang, J. Alhoee, Mixed convection of EG/NEPCM inside a lid-driven cavity with a rotating cylinder, Case Stud. Therm. Eng. 47 (2023) 103072, https://doi.org/10.1016/j.csite.2023.103072.

[23] A. Jamekhorshid, S.M. Sadrameli, M. Farid, A review of microencapsulation methods of phase change materials (PCMs) as a thermal energy storage (TES) medium, Renew. Sustain. Energy Rev. 31 (2014) 531–542, https://doi.org/10.1016/j.rser.2013.12.033.

[24] Y. Chen, Z. Yao, B. Chen, Z. Liu, C. Yang, Numerical and experimental study of the ocean thermal energy capture process utilizing metal foam–phase-change material (PCM) composites, J. Energy Storage 67 (2023) 107600, https://doi.org/10.1016/j.est.2023.107600.

[25] S. Rostami, M. Afrand, A. Shahsavar, M. Sheikholeslami, R. Kalbasi, S. Aghakhani, M.S. Shadloo, H.F. Oztop, A review of melting and freezing processes of PCM/nano-PCM and their application in energy storage, Energy 211 (2020) 118698, https://doi.org/10.1016/j.energy.2020.118698.

[26] M.M. Umair, Y. Zhang, K. Iqbal, S. Zhang, B. Tang, Novel strategies and supporting materials applied to shape-stabilize organic phase change materials for thermal energy storage–A review, Appl. Energy 235 (2019) 846–873, https://doi.org/10.1016/j.apenergy.2018.11.017.

[27] C. Zeng, Y. Yuan, F. Haghighat, K. Panchabikesan, M.M. Joybari, X. Cao, L. Klimeš, Application of PCM-based thermal energy storage system in buildings: a state of the art review on the mathematical modeling approaches and experimental investigations, J. Therm. Sci. 31 (2022) 1821–1852, https://doi.org/10.1007/s11630-022-1650-5.

[28] N. Dhaidan, H. Hashim, A. Abbas, J. Khodadadi, W. Almosawy, F. Al-Mousawi, Discharging of PCM in various shapes of thermal energy storage systems: a review, J. Therm. Sci. 32 (2023) 1124–1154, https://doi.org/10.1007/s11630-023-1793-z.

[29] A. Babapoor, G. Karimi, S. Sabbaghi, Thermal characteristic of nanocomposite phase change materials during solidification process, J. Energy Storage 7 (2016) 74–81, https://doi.org/10.1016/j.est.2016.05.006.

[30] D. Dsilva Winfred Rufuss, L. Suganthi, S. Iniyan, P.A. Davies, Effects of nanoparticle-enhanced phase change material (NPCM) on solar still productivity, J. Clean. Prod. 192 (2018) 9–29, https://doi.org/10.1016/j.jclepro.2018.04.201.

[31] M.A. Fazal, S. Rubaiee, Power output enhancement in photovoltaic systems through integration of TiO2-doped phase change material, J. Therm. Anal. Calorim. 148 (2023) 11093–11101, https://doi.org/10.1007/s10973-023-12405-9.

[32] I. Zarma, M. Ahmed, S. Ookawara, Enhancing the performance of concentrator photovoltaic systems using Nanoparticle-phase change material heat sinks, Energy Convers. Manag. 179 (2019) 229–242, https://doi.org/10.1016/j.enconman.2018.10.055.

[33] T.-P. Teng, C.-C. Yu, Characteristics of phase-change materials containing oxide nano-additives for thermal storage, Nanoscale Res. Lett. 7 (2012) 1–10, https://doi.org/10.1186/1556-276X-7-611.
[34] J.M. Mahdi, S. Lohrasbi, D.D. Ganji, E.C. Nsofor, Simultaneous energy storage and recovery in the triplex-tube heat exchanger with PCM, copper fins and Al2O3 nanoparticles, Energy Convers. Manag. 180 (2019) 949–961, https://doi.org/10.1016/j.enconman.2018.11.038.
[35] M. Bouguila, A. Samet, M.A.B. Souf, A.E. Hami, M. Haddar, Thermal performances of finned heat sink filled with nano-enhanced phase change materials: design optimization and parametric study, Int. J. Heat Mass Tran. 202 (2023) 123710, https://doi.org/10.1016/j.ijheatmasstransfer.2022.123710.
[36] A.G. Anter, A.A. Sultan, A.A. Hegazi, M.A. El Bouz, Thermal performance and energy saving using phase change materials (PCM) integrated in building walls, J. Energy Storage 67 (2023) 107568, https://doi.org/10.1016/j.est.2023.107568.
[37] M. Alam, H. Jamil, J. Sanjayan, J. Wilson, Energy saving potential of phase change materials in major Australian cities, Energy Build. 78 (2014) 192–201, https://doi.org/10.1016/j.enbuild.2014.04.027.
[38] Z. Ma, W. Lin, M.I. Sohel, Nano-enhanced phase change materials for improved building performance, Renew. Sustain. Energy Rev. 58 (2016) 1256–1268, https://doi.org/10.1016/j.rser.2015.12.234.
[39] S.Y. Wu, H. Wang, S. Xiao, D.S. Zhu, An investigation of melting/freezing characteristics of nanoparticle-enhanced phase change materials, Journal of Thermal Analysis and Calorimetry 110 (2011) 1127–1131, https://doi.org/10.1007/s10973-011-2080-x.
[40] M.-J. Li, Y.-Q. Shi, T.-Y. Lan, H.-H. Yang, G.-N. Chen, Solid-state electrochemiluminescence of two iridium(III) complexes, J. Electroanal. Chem. 702 (2013) 25–30, https://doi.org/10.1016/j.jelechem.2013.04.029.
[41] Y. Cui, C. Liu, S. Hu, X. Yu, The experimental exploration of carbon nanofiber and carbon nanotube additives on thermal behavior of phase change materials, Sol. Energy Mater. Sol. Cell. 95 (2011) 1208–1212, https://doi.org/10.1016/j.solmat.2011.01.021.
[42] S. Jesumathy, M. Udayakumar, S. Suresh, Experimental study of enhanced heat transfer by addition of CuO nanoparticle, Heat Mass Tran. 48 (2012) 965–978, https://doi.org/10.1007/s00231-011-0945-y.
[43] L. Colla, L. Fedele, S. Mancin, L. Danza, O. Manca, Nano-PCMs for enhanced energy storage and passive cooling applications, Appl. Therm. Eng. 110 (2017) 584–589, https://doi.org/10.1016/j.applthermaleng.2016.03.161.
[44] S.C. Lin, H.H. Al-Kayiem, Evaluation of copper nanoparticles – paraffin wax compositions for solar thermal energy storage, Sol. Energy 132 (2016) 267–278, https://doi.org/10.1016/j.solener.2016.03.004.
[45] A.M. Soodmand, B. Azimi, S. Nejatbakhsh, H. Pourpasha, M.E. Farshchi, H. Aghdasinia, M. Mohammadpourfard, S. Zeinali Heris, A comprehensive review of computational fluid dynamics simulation studies in phase change materials: applications, materials, and geometries, J. Therm. Anal. Calorim. 148 (2023) 10595–10644, https://doi.org/10.1007/s10973-023-12438-0.
[46] M.A. Sheik, M.K. Aravindan, N. Beemkumar, P.K. Chaurasiya, J.A. Dhanraj, Enhancement of heat transfer in PEG 1000 using nano-phase change material for thermal energy storage, Arab J Sci Eng 47 (2022) 15899–15913, https://doi.org/10.1007/s13369-022-06810-9.
[47] D.K. Mishra, S. Bhowmik, K.M. Pandey, Development and assessment of beeswax/expanded graphite composite phase change material for thermal energy storage, Arab J Sci Eng 47 (2022) 8985–9004, https://doi.org/10.1007/s13369-021-06476-9.
[48] S. Tahan Latibari, M. Mehrali, M. Mehrali, T.M.I. Mahlia, H.S.C. Metselaar, Fabrication and performances of microencapsulated palmitic acid with enhanced thermal properties, Energy Fuels 29 (2015) 1010–1018, https://doi.org/10.1021/ef502840f.
[49] A. Arasu, A. Sasmito, A. Mujumdar, Thermal performance enhancement of paraffin wax wıth Al2o3 and cuo nanopartıcles – a numerıcal study, Frontiers in Heat and Mass Transfer (FHMT) 2 (2012). https://www.thermalfluidscentral.org/journals/index.php/Heat_Mass_Transfer/article/view/137. (Accessed 27 October 2023).
[50] S. Jegadheeswaran, A. Sundaramahalingam, Synthesis and characterization of copper nanoparticles-embedded paraffin wax for solar energy storage, J. Therm. Anal. Calorim. 148 (2023) 3417–3425, https://doi.org/10.1007/s10973-023-11952-5.
[51] F. Jamil, H.M. Ali, M.A. Nasir, M. Karahan, M.M. Janjua, A. Naseer, A. Ejaz, R.A. Pasha, Evaluation of photovoltaic panels using different nano phase change material and a concise comparison: an experimental study, Renew. Energy 169 (2021) 1265–1279, https://doi.org/10.1016/j.renene.2021.01.089.
[52] S.K. Singh, S.K. Verma, R. Kumar, Thermal performance and behavior analysis of SiO2, Al2O3 and MgO based nano-enhanced phase-changing materials, latent heat thermal energy storage system, J. Energy Storage 48 (2022) 103977, https://doi.org/10.1016/j.est.2022.103977.
[53] X. Jin, X. Xu, X. Zhang, Y. Yin, Determination of the PCM melting temperature range using DSC, Thermochim. Acta 595 (2014) 17–21, https://doi.org/10.1016/j.tca.2014.09.004.
[54] L. Xingang, Q. Weilin, An improved single-plate method for measuring the thermal resistance of fibrous materials, Meas. Sci. Technol. 8 (1997) 525, https://doi.org/10.1088/0957-0233/8/5/010.
[55] A.E. Gürel, G. Yıldız, A. Ergün, İ. Ceylan, Exergetic, economic and environmental analysis of temperature controlled solar air heater system, Cleaner Engineering and Technology 6 (2022) 100369, https://doi.org/10.1016/j.clet.2021.100369.